

Charge order suppression and weak ferromagnetism in $\text{La}_{1/3}\text{Sr}_{2/3}\text{FeO}_3$ nanoparticles

F. Gao, P. L. Li, Y. Y. Weng, S. Dong, L. F. Wang, L. Y. Lv, K. F. Wang, and J.-M. Liu^{a)}
*Laboratory of Solid State Microstructures, Nanjing University, Nanjing 210093, China and
 International Center for Materials Physics, Chinese Academy of Sciences, Shenyang 110016, China*

Z. F. Ren

Department of Physics, Boston College, Chestnut Hill, Massachusetts 02467

(Received 5 April 2007; accepted 14 July 2007; published online 14 August 2007)

Perovskite-type polycrystalline $\text{La}_{1/3}\text{Sr}_{2/3}\text{FeO}_3$ particles with different sizes (80–2000 nm) were prepared using a simple sol-gel technique. In samples of nanoparticles with a diameter of less than 300 nm, weak ferromagnetism was observed at room temperature, which was attributed to the lattice distortion. The magnetic and specific heat measurements suggest that the charge ordering state was largely suppressed due to the lowering of the particle size, but the charge ordering temperature remained unaffected. © 2007 American Institute of Physics. [DOI: 10.1063/1.2768895]

The charge ordering (CO) phenomenon in transition-metal oxides has become a subject of intensive research in the last decade, because this intriguing phenomenon exhibits a close inter-relation among magnetic ordering, electronic transport, and crystal structure.^{1–16} Up until now, it has been widely recognized that the CO state is caused by the coupling or competition among charge, spin, lattice, and orbit. More recently, some CO insulators were even discussed as multiferroics, since CO induced electric polarization in them.²

Among all the CO transition-metal oxides, perovskite manganites and ferrites attracted the most attention. In manganites, giant magnetoresistance also originates due to the melting of the CO state into the ferromagnetic state by a magnetic field.³ Furthermore, in the last two years, dramatic changes in the CO state, as well as emerging magnetism, were reported in many nanosized manganites, such as $\text{Pr}_{0.5}\text{Ca}_{0.5}\text{MnO}_3$ nanowires,⁴ $\text{Nd}_{0.5}\text{Ca}_{0.5}\text{MnO}_3$ nanoparticles,⁵ $\text{Pr}_{1/2}\text{Sr}_{1/2}\text{MnO}_3$ nanoparticles,⁶ $\text{Pr}_{0.65}\text{Ca}_{0.35}\text{MnO}_3$ nanoparticles,⁷ etc.⁸ A simple theoretical model based on the surface phase separation was proposed to explain these changes.⁹

As for the perovskite ferrites with Fe in an unusually high valence state of Fe^{4+} (d^4), the CO often accompanies both antiferromagnetic (AFM) and charge disproportionation (CD) of $2\text{Fe}^{4+} \rightarrow \text{Fe}^{3+} + \text{Fe}^{5+}$, e.g., $\text{La}_{1/3}\text{Sr}_{2/3}\text{FeO}_3$ (LSFO) with CO transition point (T_{CO}) at about 200 K.¹ There are extensive experimental studies on LSFO in terms of photoemission,¹⁰ Mössbauer spectroscopy,¹¹ neutron diffraction,¹² transmission electron microscopy,¹³ optical spectroscopy,¹⁴ ultrasonic techniques,¹ etc. Takano *et al.* was the first to reveal, using Mössbauer spectroscopy, that there are two kinds of Fe ions ($\text{Fe}^{3+}:\text{Fe}^{5+}=2:1$) in LSFO.¹¹ This CD state was confirmed by the neutron powder diffraction measurements.¹² Although no lattice distortion was detected accompanying the CO/CD state by neutron diffraction, recent ultrasonic research on LSFO revealed that the electron-phonon coupling via the Jahn-Teller effect indeed exists in LSFO.¹ More recently, inelastic neutron scattering results

showed that the magnetic interactions alone are sufficient for stabilizing the CO structure in LSFO.¹⁵ However, despite these efforts, there has been no report about the CO state and magnetic properties in nanosized LSFO. In this letter, we synthesize LSFO particles with different sizes by a sol-gel method, and characterize their magnetic and specific heat properties to understand the CO state changes.

Iron nitrate [$\text{Fe}(\text{NO}_3)_3 \cdot 9\text{H}_2\text{O}$], lanthanum nitrate [$\text{La}(\text{NO}_3)_3$], and strontium nitrate [$\text{Sr}(\text{NO}_3)_2$] in stoichiometric proportions (3:1:2 molar ratio) were dissolved in 2-methoxyethanol ($\text{C}_3\text{H}_8\text{O}_2$). Then citric acid, in 1:1 molar ratio with respect to the metal nitrates, was added to the solution as a complexant, followed by polyethylene glycol as a dispersant. The mixture was stirred for about an hour at 80 °C to obtain the sol, which was then kept at 80 °C for 4 days to form the dried gel powder. In order to obtain LSFO particles with different sizes, the final powder was calcined at different temperatures of 1000–1300 °C for different times of 1–2 h.

The morphology and structure of the LSFO particles were investigated by scanning electron microscopy (SEM), transmission electron microscopy (TEM), and x-ray diffraction (XRD). The specific heat was performed from 160 to 230 K. A superconducting quantum interference device magnetometer was employed to characterize the magnetization (M) as a function of temperature (T) and magnetic field (H).

The typical SEM images of the LSFO particles are shown in Figs. 1(a)–1(d), which represents the samples calcined at 1000 °C for 2 h, 1100 °C for 2 h, 1200 °C for 1 h, and 1300 °C for 2 h. From the images, we can see that these particles have an average size of about 80, 200, 300, and 2000 nm, respectively. In the following, we designate these samples as LSFO-80, LSFO-200, LSFO-300, and LSFO-2000, respectively. There is a dramatic change in size between LSFO-300 and LSFO-2000, and the latter is close to the size of bulk LSFO. The inset of Fig. 1(a) is a representative TEM picture of the LSFO-80 sample, which shows the presence of the single isolated nanoparticles of size about 80 nm, in addition to the aggregated nanoparticles. Figure 1(e) is the high-resolution TEM (HRTEM) image of the LSFO-80 nanoparticle as well as the selected area electron diffraction pattern (inset). Both of them confirm that our

^{a)} Author to whom correspondence should be addressed; electronic mail: liujm@nju.edu.cn

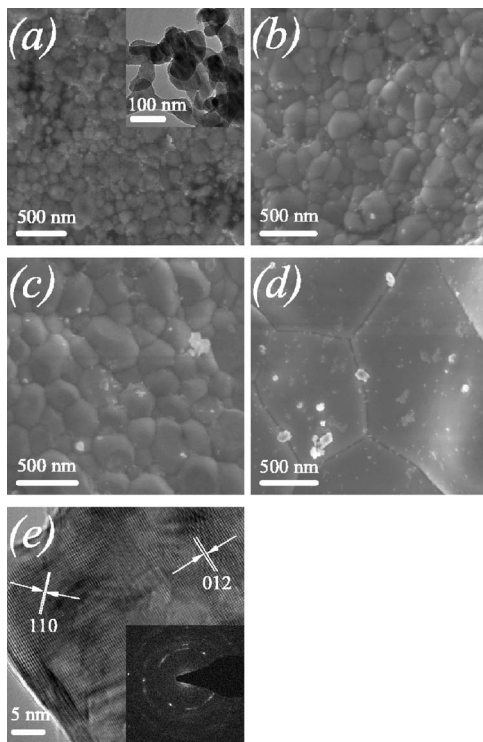


FIG. 1. (a) SEM image of LSFO particles calcined at 1000 °C for 2 h with the TEM image as the inset. (b) SEM image of LSFO particles calcined at 1100 °C for 2 h. (c) SEM image of LSFO particles calcined at 1200 °C for 1 h. (d) SEM image of LSFO particles calcined at 1300 °C for 2 h. (e) HRTEM image of LSFO particles calcined at 1000 °C for 2 h with the SAED pattern in the inset.

LSFO nanoparticles are well crystallized with a single-phase perovskite structure.

Figure 2(a) presents the XRD pattern of the LSFO particles calcined at different temperatures for different times.

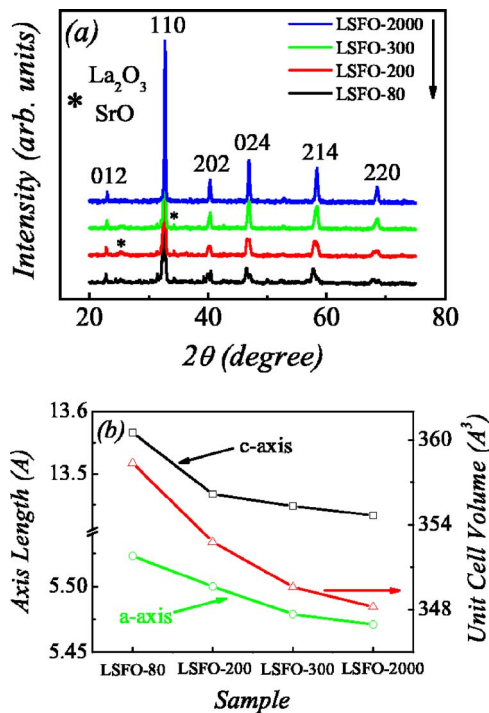


FIG. 2. (Color online) (a) XRD pattern of LSFO particles with different particle sizes. (b) *a*- and *c*-axis constants and the unit cell volume of different particles.

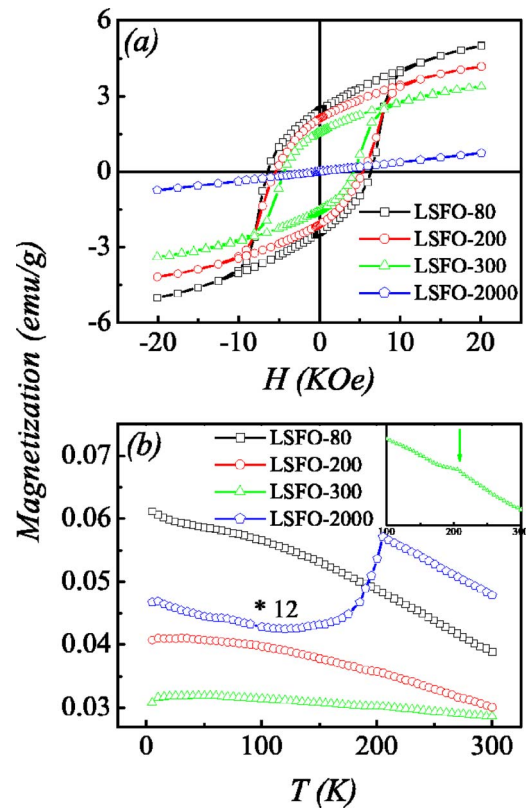


FIG. 3. (Color online) (a) *M-H* hysteresis loops of the LSFO particles measured at room temperature. (b) *M-T* curves for LSFO particles measured at ZFC condition; inset is the partially enlarged curve of LSFO-300.

All the diffraction peaks can be indexed with the space group $R\bar{3}c$ in the hexagonal setting, well matched with the structure of bulk LSFO,¹⁶ except for two tiny peaks, which can be indexed as La_2O_3 or SrO . Furthermore, the hexagonal lattice constants evaluated from the XRD spectra are summarized in Fig. 2(b), as a function of different samples. Slight expansion in both the *ab* plane and the *c* axis with decreasing particle size from 2000 to 80 nm is clearly seen, resulting in the increase of the unit cell volume. The volume of LSFO-2000 is 348.20 \AA^3 , the same as that of bulk LSFO within the experiment error.¹⁶ We also performed x-ray photoelectron spectroscopy (XPS) measurements on all the samples (not shown here), and found that the $\text{Fe}2p_{3/2}$ core levels lie almost at the same binding energy for all the samples, which indicated that there was no difference in the Fe ion state for the samples sintered at different temperatures.

Figure 3(a) shows the size dependent magnetization of LSFO particles at room temperature (RT). LSFO-2000 is paramagnetic, consistent with the RT magnetic behavior of LSFO bulk.¹ However, LSFO-80, LSFO-200, and LSFO-300 all show obvious, though weak, ferromagnetic (FM) behavior. Many experimental results on nanosized manganites also showed that the nanosize could lead to the emergence of FM, which was attributed to the suppression of CO, hence appearing below T_{CO} .⁴⁻⁸ However, the FM behavior in our LSFO particles emerged at RT, a temperature much higher than T_{CO} (around 200 K). Therefore, there might be another mechanism for this behavior. It is well acknowledged that the lattice distortion may bring significant changes to the characters of materials.¹⁷ In LSFO, the distortion of the lattice could cause considerable changes in the angle and length of Fe-O bond, and consequently affects the magnetic structure of

LSFO greatly. Therefore, we suggest that the emergence of weak FM in nanosized LSFO is attributed to the obvious expansion of the a and c axes as well as the volume [Fig. 2(b)]. In fact, Yang *et al.* have observed the weak FM in bulk LSFO at low temperature, together with the lattice distortion at the same time.¹⁶ From a broader scope, in AFM systems, a parasitic FM component is often observed as a result of the lattice distortion, e.g., BiFeO₃,¹⁸ La_{0.875}Sr_{0.125}MnO₃,¹⁹ etc. We have also estimated the FM component, using the value of magnetization at the highest field available to us (2 T). We got $0.127\mu_B/\text{Fe}$ for LSFO-300, $0.156\mu_B/\text{Fe}$ for LSFO-200, and $0.187\mu_B/\text{Fe}$ for LSFO-80. Compared with the expected value of $2.4\mu_B/\text{Fe}$,¹⁶ the FM component only occupied 5.3%, 6.5%, and 7.8%, respectively. These results are comparable with the FM component in distorted AFM BiFeO₃ nanoparticles.¹⁸ In addition, we notice that the coercive field of these samples is quite large, which makes them promising candidates in general memory devices, in addition to the specific application at RT, involving spintronics and spin valves.²⁰

We also measured M (at $H=100$ Oe) as a function of T for all the samples under the zero-field-cooling (ZFC) condition, as shown in Fig. 3(b). In order to present all the data in one figure, we multiplied the magnetization of LSFO-2000 by 12. It is well known that the CO transition is characterized by a peak in the magnetization where double exchange is suppressed due to the localization of the charge carriers, resulting in a large drop of susceptibility.²¹ The LSFO-2000 sample shows the CO peak at around 200 K, which coincides with the previous results on bulk LSFO.¹ However, for LSFO-300, the CO induced magnetization drop around 200 K is greatly suppressed, though still present, as shown in the inset. It means that when the particle size is as large as 300 nm, the CO in LSFO is already largely destroyed. As for LSFO-200 and LSFO-80, the drop around 200 K is entirely absent, which shows that with the decrease of particle size, the CO in LSFO is suppressed further. In LSFO, superexchange interactions are AFM between Fe³⁺ and Fe³⁺ (J_{AF}) and FM between Fe³⁺ and Fe⁵⁺ (J_{F}).¹⁵ McQueeney *et al.* have pointed out that the CO state in LSFO is determined by the ratio between J_{F} and J_{AF} , analyzed from the inelastic neutron scattering result.¹⁵ Since the lattice distortion affects J_{F} and J_{AF} , we consider that distortion is responsible for the suppression of CO in nanosized LSFO. Although both the a axis and c axes were expanded and the influence on J_{F} and J_{AF} will be similar, the extent to which J_{F} and J_{AF} are affected is possible to be different, resulting in different ratios between J_{F} and J_{AF} , compared with undistorted LSFO. Therefore, a suppression of the charge ordered state caused by the a - and the c -axis expansion is possible.

In order to further characterize the CO in LSFO particles, specific heat measurement was performed on all the samples. As shown in Fig. 4, a very obvious peak was observed around 200 K for LSFO-2000, which agrees well with earlier reports.¹ As the particle size decreases from 2000 to 300 nm, the specific heat peak lies at almost the same temperature, but the intensity is much weaker, which means that CO is partly destroyed. With the further decrease of the particle size from 300 to 200 nm, the CO induced peak is further weakened but still present. This behavior seems to contradict with the fact that the CO induced magnetization drop around 200 K is invisible in the M - T curve of LSFO-200. We consider the reason as follows: since the

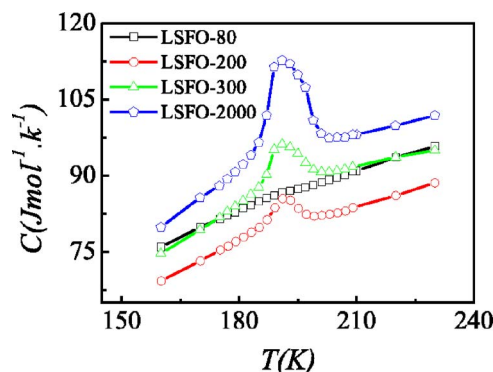


FIG. 4. (Color online) Temperature dependent specific heat measurement of different LSFO particles.

CO state is only partly destroyed in LSFO-200, as indicated in the specific heat measurement, there ought to be a drop in the M - T curve. But considering that LSFO-200 has become ferromagnetic, it is highly possible that the drop is covered up by the enhanced magnetization. When the particle size reaches 80 nm, the specific heat peak nearly disappears, indicating that CO in LSFO is almost totally destroyed when the particle is 80 nm.

This work was supported by the National Natural Science Foundation of China (50332020, 50528203, and 50601013), the National Key Project for Basic Research of China (2002CB921802), the 111 Project of MOE of China, and the Scientific Research Foundation of Nanjing University (2006CL01).

¹H. Kong and C. Zhu, Appl. Phys. Lett. **88**, 041920 (2006).

²S. W. Cheong and M. Mostovoy, Nat. Mater. **6**, 13 (2007).

³A. P. Ramirez, S.-W. Cheong, and P. Schiffer, J. Appl. Phys. **81**, 5337 (1997).

⁴S. S. Rao, K. N. Anuradha, S. Sarangi, and S. V. Bhat, Appl. Phys. Lett. **87**, 182503 (2005).

⁵S. S. Rao, S. Tripathi, D. Pandey, and S. V. Bhat, Phys. Rev. B **74**, 144416 (2006).

⁶A. Biswas, I. Das, and C. Majumdar, J. Appl. Phys. **98**, 124310 (2005).

⁷A. Biswas and I. Das, Phys. Rev. B **74**, 172405 (2006).

⁸Z. Q. Wang, F. Gao, K. F. Wang, H. Yu, Z. F. Ren, and J.-M. Liu, Mater. Sci. Eng., B **136**, 96 (2007).

⁹S. Dong, F. Gao, Z. Q. Wang, J.-M. Liu, and Z. F. Ren, Appl. Phys. Lett. **90**, 082508 (2007).

¹⁰J. Matsuno, T. Mizokawa, A. Fujimori, K. Hamiya, Y. Takeda, S. Kawasaki, and M. Takano, Phys. Rev. B **60**, 4605 (1999).

¹¹M. Takano, J. Kawachi, N. Nakanishi, and Y. Takeda, J. Solid State Chem. **39**, 75 (1981).

¹²P. D. Battle, T. C. Gibb, and P. Lightfoot, J. Solid State Chem. **84**, 271 (1990).

¹³J. Q. Li, Y. Matsui, S. K. Park, and Y. Tokura, Phys. Rev. Lett. **79**, 297 (1997).

¹⁴T. Ishikawa, S. K. Park, T. Katsufuji, T. Arima, and Y. Tokura, Phys. Rev. B **58**, R13326 (1998).

¹⁵R. J. McQueeney, J. Ma, S. Chang, J.-Q. Yan, M. Hehlen, and F. Trouw, Phys. Rev. Lett. **98**, 126402 (2007).

¹⁶J. B. Yang, X. D. Zhou, Z. Chu, W. H. Hikal, Q. Cai, J. C. Ho, D. C. Kundaliya, W. B. Yelon, W. J. James, H. U. Anderson, H. H. Hamdeh, and S. K. Malik, J. Phys.: Condens. Matter **15**, 5093 (2003).

¹⁷M. Coey, Nature (London) **430**, 155 (2004).

¹⁸F. Gao, X. Y. Chen, K. B. Yin, S. Dong, Z. F. Ren, F. Yuan, T. Yu, Z. G. Zou, and J.-M. Liu, Adv. Mater. (Weinheim, Ger.), 10.1002/adma.200602377 (in press).

¹⁹D. N. Argyriou, J. F. Mitchell, C. D. Potter, D. G. Hinks, J. D. Jorgensen, and S. D. Bader, Phys. Rev. Lett. **76**, 3826 (1996).

²⁰J. Dho, X. Qi, H. Kim, J. L. MacManus-Driscoll, and M. G. Blamire, Adv. Mater. (Weinheim, Ger.) **18**, 1445 (2006).

²¹F. Millange, S. de Brion, and G. Chouteau, Phys. Rev. B **62**, 5619 (2000).